Preliminary Performance Analysis of a Prototype DFMC SBAS Service over Australia and Asia-Pacific

Jizhong Wu[1,2], Kan Wang *[1], Ahmed El-Mowafy[1]

[1] *School of Earth and Planetary Sciences, Curtin University, GPO Box U1987, Perth, WA, Australia*

[2] *School of Geomatics Science and Technology, Nanjing Tech University, 211816, Nanjing, China*

Abstract:

The next-generation of satellite-based augmentation system (SBAS) will employ a dual-frequency multi-constellation (DFMC) service providing several advantages over the classical SBAS L1 service. In September 2017, a two-year SBAS test-bed was initiated by Australia and New Zealand in preparation for building an operational system. This system includes DFMC SBAS in addition to the legacy SBAS L1 service and real-time precise point positioning (PPP) service over the Asia-Pacific region. In this paper, we focus on the new DFMC SBAS, and first discuss its positioning and integrity monitoring (IM) algorithms. Next, its performance is tested and analyzed using real DFMC SBAS data, restricting focus to LPV-200 in aviation. Based on real SBAS messages from the geostationary (GEO) satellite Inmarsat-4F1, testing was performed first at two known stations with actual GNSS observations, and next at simulated grids covering the entire Asia-Pacific region. A sensitivity analysis is performed, investigating the contribution of the error sources and the impact of changing the satellite mask angle. Experimental results of 12 consecutive days from September 14 to 25, 2018 of the new SBAS products show that the dual-frequency correction (DFC) residual errors have the dominant contribution in the values of the protection levels needed in IM, whereas other error sources such as the airborne receiver errors, the tropospheric and the ionosphere residual errors have secondary impacts. The accuracy of the positions was found to be at the sub-meter to meter level and was always bounded by the protection levels (PLs) at the known stations. The simulated PLs were less than the alert limit of LPV-200 during the test period in most of the areas of interest, indicating the availability of IM using DFMC SBAS in the main areas of the Asia-pacific region.

Keywords: SBAS; DFMC; GPS; Galileo; Integrity; Protection level; Availability

1. Introduction

The GNSS-based positioning service has been widely used in a variety of safety-of-life aeronautical applications, including the aircraft precision approach and automatic landing. In these applications, integrity measures are essential to indicate the trust that can be placed in the correctness of the navigation information. IM provides timely and valid warnings to the navigation users when the system fails to be used for the intended operation. However, a stand-alone navigation system is vulnerable to constellation weakness. The combined usage of ranging signals from multiple GNSS constellations has thus been taken into consideration (Walter et al, 2014; El-Mowafy and Yang, 2016).

* Corresponding author, E-mail: kan.wang@curtin.edu.au

Classical SBAS was primarily developed to improve the position accuracy, the service availability and the integrity performance of the aeronautical applications through introducing external range, orbit, clock and ionospheric corrections into the positioning process (Wanner et al., 2008). It is used to support better positioning service than single point positioning (SPP) and provide integrity information in civil aviation for nearly two decades. Examples start with the Wide Area Augmentation System (WAAS) of the United States, which is followed by the Multi-functional Satellite Augmentation System (MSAS) of Japan, the European Geostationary Navigation Overlay Service (EGNOS), and the Geo-Augmented Navigation system (GAGAN) of India. These four systems provide a GPS-only single-frequency positioning service over L1 (Choy et al., 2017). As these SBASs augment only single-frequency measurements, the ionosphere delays need to be processed and delivered to the users. This makes single-frequency SBAS sensitive to the distribution of the ground network used to compute the ionosphere corrections, have a limited coverage area, and are less precise during rapid fluctuations of the ionosphere.

Rather than relying on the SBAS ionospheric grid, adding a second frequency, e.g. L5, as applied in the second-generation SBAS, directly removes the majority of the ionospheric delays. Furthermore, the multi-constellation scenario will profoundly increase the number of satellites provide users with better measurement geometry. By 11 May 2020, there are 14 operational GPS IIF and III satellites transmitting signals on L1 and L5, and the DFMC scenario adds 22 Galileo satellites transmitting signals on E1 and E5a. The number of satellites will continue to increase in the future with the planned lunch of new GPS and Galileo satellites. An initial study indicates that even when using the GPS L1/L2 signals due to the currently limited GPS satellites sending L5 signals, the mean PLs of the DFMC SBAS can be improved by more than 24% compared to L1 SBAS legacy service (Barrios et al., 2018). As a result, the single-constellation single-frequency SBAS is evolving towards the new generation in the entire world. EGNOS, for example, plans to augment both GPS and Galileo on both their L1 and L5 signals (Teunissen and Montenbruck, 2017; Salos et al., 2018), and WAAS is also preparing for the dual-frequency operations (Walter et al., 2012a; 2012b; Bunce, 2014).

Starting from 2017, Australia and New Zealand initiated a second-generation SBAS test-bed to evaluate the performance, safety, productivity and innovation benefits of SBAS in different industries and research sectors (Geoscience Australia, 2017, Wang et al., 2020). The test-bed continuously broadcasts three services, i.e., the SBAS L1 legacy service that is consistent with current SBAS equipment, the future SBAS L5 DFMC service and the real-time precise point positioning (PPP) (Zumberge et al., 1997) service transmitted through L1 and L5 (Barrios et al., 2018; El-Mowafy et al., 2019). Such an SBAS program plays a leading role in providing such a diverse range of advanced services. Although the focus of this study is put on the DFMC SBAS service, it is worthwhile to be mentioned the new SBAS test-bed also supports the PPP service by broadcasting precise satellite orbit and clock information to users via L1 and L5. The PPP corrections sent through L1 support the GPS dual-frequency users, and those sent through L5 support the GPS/Galileo dual-frequency users.

In this work, we restrict our attention to the DFMC SBAS service, which has several notable differences to the L1 SBAS legacy service. First, as mentioned before, the DFMC SBAS service exploits the L1 and L5 observations from GPS and E1/E5a from Galileo satellites to

remove the first-order ionospheric delays through forming the ionosphere-free combination. This releases the system from computing and transmitting the ionospheric corrections to users. The residual high-order terms of the ionospheric errors have a magnitude of centimeters even under extreme conditions (Pireaux et al., 2010), which is considered in the IM process. Second, the vertical service coverage area will not be restricted to the region for which the ionospheric corrections are computed, and can be expanded to the entire foot-print of the geostationary (GEO) satellite transmitting SBAS. During the test-bed, Inmarsat-4F1 located at the 143.5°E longitude was used for this purpose. Besides, as mentioned earlier, the use of measurements from two constellations improves the satellite geometry and thus would improve the positioning precision.

In addition to providing measurement corrections, SBAS enables IM that checks whether the navigation system meets the integrity requirements for a given operation and aims to bound the positioning errors with certain protection levels (PL) under a pre-set probability of hazardous misleading information (PHMI) according to the application at hand. The aviation communities, such as the International Civil Aviation Organization (ICAO) and the Radio Technical Commission for Aeronautics (RTCA), have developed a range of mathematical models to monitor the integrity of the positioning service in aviation (Roturier et al., 2001; RTCA, 2016). Some studies investigated the PLs for GPS L1 or simulated GPS L1/L5 dual-frequency SBAS (Blanch et al., 2005; Wanner et al., 2008; Grunwald et al., 2016; Walter et al., 2007; Walter et al., 2010). Studies on the integrity performance of the DFMC SBAS service, in particular using actual data and with the up-to-date algorithms, are lacking. This is the focus of this contribution, investigating the influence of individual error sources on protection levels, presenting and analyzing the performance IM from DFMC SBAS service for aeronautical applications, in particular, that are based on the Australian and New Zealand SBAS test-bed data. The requirements of Localizer Performance with Vertical guidance (LPV) approach down to 200 feet (known as LPV-200) are considered.

The paper starts with an overview of the architecture of the DFMC SBAS test-bed, as well as its message types, observation model and the protection level algorithm used in the DFMC SBAS service. This is followed by data analysis based on real DFMC SBAS data and GNSS observations at two known stations and at a simulated grid covering the whole Asia-Pacific region to illustrate the DFMC SBAS integrity performance. The factors affecting values of the protection levels and the vertical positioning availabilities are investigated. The conclusion is given at the end of the paper.

2. Architecture and message type of the DFMC SBAS test-bed

As illustrated in Figure 1 (left panel), the DFMC SBAS infrastructure comprises the space segment, the ground segment, the user segment and the support segment. The space segment refers to the GPS and Galileo satellites in addition to the GEO satellite Inmarsat-4F1 (PRN 122). The ground segment consists of the monitoring station network, the Augmentation Processing Center (APC) and the uplink system at Uralla in New South Wales, Australia. The support segment is a web-based tool used to monitor the operation and maintenance of the system. In the ground segment, raw GNSS observations are collected from a global network consisting of stations in, e.g., the International GNSS Service (IGS) (Johnston et al., 2017), the

Australian Regional GNSS Network (Twilley and Digney, 2001), the LINZ PositioNZ network (LINZ, 2020), and the South Pacific Regional GNSS network (Deo and Twilley, 2008). The collected observations at each monitoring station are transferred to the APC, which computes the SBAS message including corrections and integrity information, and sends them to the uplink system. Finally, SBAS messages are transformed into electromagnetic signals and sent to the GEO satellite via the uplink system. The test-bed exploits a worldwide monitoring station network. The red hexagrams in Figure 1 (right panel) shows the distribution of these reference stations (Barrios et al., 2018) and the coverage area of the test-bed.

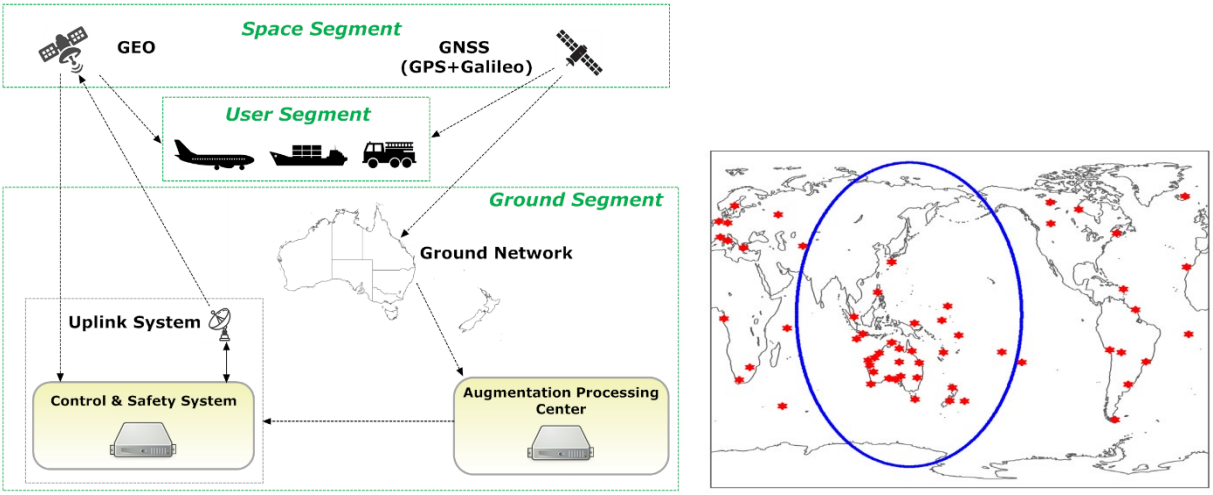

Fig. 1 SBAS test-bed architecture (left) and DFMC SBAS service coverage areas (right)

At an altitude of about 36,000 km, the GEO satellite Inmarsat-4F1 transmits SBAS messages to users in an extended coverage area. Figure 1 (right panel) illustrates the coverage area of Inmarsat-4F1 when the elevation mask is set to 5 degrees. Users within the area bounded by blue elliptical shape are expected to receive the DFMC SBAS messages, which are transmitted at a data rate of 250 bits per second (bps). Every message consists of 250 bits composed of a 4-bit preamble, a 6-bit message type identifier, a 216-bit data field, and a 24-bit cyclic redundancy check (EUROCAE, 2019). The difference in data block format between the DFMC and the legacy L1 signals lies in the length of the preamble and the data field, which are 8 bits and 212 bits, respectively, for the SBAS L1 legacy message. In addition, the message identifiers for DFMC SBAS are different from those of SBAS L1 Legacy. The main message types associated with computing the position and the protection levels for DFMC SBAS are given in Table 1. The second last column of Table 1 gives the percentage of each message type according to the statistics of real DFMC SBAS messages from September 14 to September 25, 2018. It can be seen that message type 32 makes up a large proportion of the DFMC SBAS messages, as every message of type 32 contains the corrections parameters for a single satellite.

Table 1 Message types for DFMC SBAS

Message Type	Contents	Percentage	Average update interval (s)
31	Satellite mask assignments	1.96%	51.1
34, 35, 36	Integrity information	18.07%	5.9/181.7/220.5
32	Satellite clock & ephemeris error corrections and covariance matrix, integrity	74.45%	1.3

	information		
37	Old but active data (OBAD) parameters and dual-frequency range error indicator (DFREI) scale table	0.98%	101.85

3. DFMC SBAS positioning and protection levels

In IM, the positioning errors should be bounded by the protection levels, defined in the horizontal and vertical directions as the horizontal protection level (HPL) and the vertical protection level (VPL). During operation, these protection levels are computed at each time epoch and are compared to the application-dependent alert limit (AL). If the PL> AL, a warning should be sent to the user within a pre-defined time-to-alert period, e.g. 6 seconds. Currently, the IM algorithms for DFMC SBAS are in the testing and standardization phase and very little is published in the literature on these algorithms. This section summarizes the observation model and the algorithm of computing the protection levels used in this study. It is based on the latest minimum operational performance standards (MOPS) specified by the European Organization for Civil Aviation Equipment (EUROCAE), as given in the document ED-259 (EUROCAE, 2019). The focus is restricted to SBAS application of LPV-200 in aviation.

3.1 Observation model

The DFMC SBAS service within the SBAS test-bed makes use of both the L1/L5 GPS and the E1/E5 Galileo code observations. To reduce the large code noise and thus achieve a higher positioning precision, the code observations are smoothed by the carrier-phase observations using the following filter:

$$p_t = \alpha \frac{\rho_{5,t} - \gamma \cdot \rho_{1,t}}{1-\gamma} + (1-\alpha)\left[p_{t-1} + \frac{\lambda_5 \cdot \Delta\varphi_{5,t} - \gamma \cdot \lambda_1 \cdot \Delta\varphi_{1,t}}{2\pi(1-\gamma)}\right] \quad (1)$$

where p_t is the carrier-smoothed pseudorange observations at time t, α is the filter weighting function related to the filter time and sample interval, ρ is the raw pseudorange measurement in meters with two subscripts identifying the carrier frequency and the epoch respectively, γ is a constant denoting the square of the L1/L5 and E1/E5a frequency ratios, $\Delta\varphi$ is the difference of raw carrier-phase measurement in radians between epoch t and t-1, i.e., $\Delta\varphi_{5,t} = \varphi_{5,t} - \varphi_{5,t-1}$, here the subscripts have the same interpretation as with ρ. λ is the wavelength in meters with the subscript representing the carrier frequency.

Assuming that the number of usable GPS and Galileo satellites is m and n, respectively, at a single epoch the multi-constellation observation model can be formulated as

$$y = Ax + e \quad (2)$$

where y is (m+n) vector containing observed-minus-computed (O-C) observations, i.e., $y = p - \tilde{\rho}$, the differences between the ionosphere-free smoothed pseudorange measurements (p) and the expected observations ($\tilde{\rho}$). The 5×1 vector $\boldsymbol{x}$ contains the 3D receiver position increments (starting from an initial position), in addition to the GPS and the Galileo receiver clock offsets. The term $\boldsymbol{e}$ is the measurement error vector. The design matrix $\boldsymbol{A}$ is of dimension

m+*n* by 5, with the *i*-th row defined as

$$A_i = [-\cos\theta_i \sin\alpha_i \quad -\cos\theta_i \cos\alpha_i \quad -\sin\theta_i \quad n_{i,G} \quad n_{i,E}] \tag{3}$$

where θ_i and α_i refers to the satellite elevation and azimuth angle for the *i*-th satellite, respectively. $n_{i,G}$ and $n_{i,E}$ are the coefficients for the GPS and Galileo receiver clocks. If the *i*-th satellite belongs to the GPS constellation, then $n_{i,G} = 1$ and $n_{i,E} = 0$. if for Galileo, $n_{i,G} = 0,$ and $n_{i,E} = 1$.

The expected observations $\tilde{\rho}$ used in computation y for a single GPS or Galileo satellite is given as

$$\tilde{\rho} = \hat{\rho} - (\tau + \Delta\tau) + TRP \tag{4}$$

for which $\hat{\rho}$ denotes the geometric range computed based on the approximate receiver coordinates and the satellite orbits corrected by SBAS. τ represents the satellite clock offset and the relativistic effects computed based on the broadcast ephemeris, and $\Delta\tau$ is the SBAS satellite clock error correction. *TRP* denotes the tropospheric delays derived from empirical models. All these terms are expressed in the unit of distance. For the GPS satellites, group delays should also be taken into consideration when using the L1/L5 signals. The satellite clock error correction $\Delta\tau$ at time *t* can be calculated as follows:

$$\Delta\tau = \Delta B + \Delta\dot{B} \ (t - t_D) \tag{5}$$

where ΔB denotes the clock offset correction in meters, and $\Delta\dot{B}$ is the clock drift correction in meter per second. t_D is the applicable time of these corrections, the orbit and clock corrections are added to the broadcast satellite orbit and clock offsets computed from the broadcast ephemeris. The SBAS orbit corrections are similarly computed based on 3D offset and drift vectors. The corresponding corrections are suggested to be broadcast in the SBAS message type 32.

The satellite measurements are screened for fault detection and exclusion (FDE), where a chi-square statistic is computed as follows:

$$\chi^2 = y^T \left(Q_y^{-1} - Q_y^{-1} A \left(A^T Q_y^{-1} A \right)^{-1} A Q_y^{-1} \right) y \tag{6}$$

The test threshold T_{χ^2} is defined by

$$F\left(T_{\chi^2}, k\right) = 1 - P_{FA} \tag{7}$$

where P_{FA} is the probability of false alert allocated to the chi-square test, for aviation application, $P_{FA} = 10^{-8}$. k is the number of redundant observations. F is the cumulative distribution function (CDF) of a chi-square distribution. If $\chi^2 > T_{\chi^2}$, a fault is suspected, and the test is re-performed by excluding one measurement at a time until the test passes.

The unknown vector *x* is next estimated by applying a weighted least-squares adjustment:

$$\hat{x} = \left(A^T Q_y^{-1} A \right)^{-1} A^T Q_y^{-1} y \tag{8}$$

where the hat (^) denotes the estimated quantity, with the variance-covariance matrix of the O-

C observation terms represented with a diagonal matrix Q_y, assuming that the error sources among different satellites are uncorrelated, such that:

$$Q_y = \mathrm{diag}(\sigma_1^2, \cdots, \sigma_{m+n}^2) \tag{9}$$

for which m and n are the numbers of satellites passing the FDE. The element σ_i^2 is the variance of the O-C observation term for the i^{th} satellite, which is expressed as:

$$\sigma_i^2 = \sigma_{DFC,i}^2 + \sigma_{ION,i}^2 + \sigma_{TRP,i}^2 + \sigma_{AIR,i}^2 \tag{10}$$

for which $\sigma_{DFC,i}^2$, $\sigma_{ION,i}^2$, $\sigma_{TRP,i}^2$, $\sigma_{AIR,i}^2$ are the variance of the DFC residual errors, the variance of the ionospheric residual errors, the variance of the tropospheric residual errors, and variance of the airborne receiver errors, respectively. Within (10), σ_{DFC}^2 is derived from the parameters broadcast in SBAS suggested message types 32, 34, 35, 36 and 37, whereas σ_{ION}^2, σ_{TRP}^2 and σ_{AIR}^2 are computed with empirical models in terms of the satellite elevation angle. Further details on these empirical models can be found in EUROCAE (2019). Note that although DFMC eliminates the first-order ionospheric delays, the parameter σ_{ION} accounts for the ionospheric residual errors of the high-order ionospheric effects, the ray-bending effects and the excess total electron content (TEC) errors. The airborne receiver errors comprise the receiver noise, the multipath and the uncertainly of the antenna group delays.

3.2 Protection levels

Since the position errors (defined as the difference between the estimated position and the true position) are not known in real practice, the HPL and VPL are computed to bound possible horizontal and vertical positioning errors under the pre-defined PHMI. Assuming that the horizontal and vertical positioning errors can be described by a zero-mean normal distribution, the HPL and VPL for DFMC SBAS are computed as

$$\begin{cases} HPL = K_H \times \sigma_{major} \\ VPL = K_V \times \sigma_{uu} \end{cases} \tag{11}$$

where σ_{major} denotes the standard deviation along the semi-major axis of the horizontal position error ellipse, which can be expressed as:

$$\sigma_{major} = \sqrt{\frac{\sigma_{ee}^2 + \sigma_{nn}^2}{2} + \sqrt{\left(\frac{\sigma_{ee}^2 - \sigma_{nn}^2}{2}\right)^2 + \sigma_{en}^2}} \tag{12}$$

where σ_{ee}, σ_{nn}, σ_{uu} and σ_{en} are the standard deviations of the east, north and up coordinates, and the covariance between east and north, derived from the variance-covariance matrix of the estimated unknowns, computed as $Q_{\hat{x}\hat{x}} = \left(A^T Q_y^{-1} A\right)^{-1}$.

The K_H and K_V amplification factors are computed based on the selected PHMI as follows:

$$\begin{cases} K_H = \phi^{-1}\left(1 - \frac{\mathrm{PHMI}_H}{2}\right) \\ K_V = \phi^{-1}\left(1 - \frac{\mathrm{PHMI}_V}{2}\right) \end{cases} \tag{13}$$

where ϕ^{-1} is the inverse CDF of the standard normal distribution, PHMI_H and PHMI_V represent the PHMI allocated to the horizontal and vertical components, respectively. In general, the integrity budgets for various operations, such as the en-route, terminal, approach lateral navigation (LNAV), approach lateral navigation/vertical navigation (LNAV/VNAV), approach localizer performance without vertical guidance (LP) and approach localizer performance with vertical guidance (LPV), have been quantified with the required probability (RTCA, 2016). More specifically, as to DFMC SBAS IM, K_H is set to be 6.18 for the LNAV application and 6.0 for the LNAV/VNAV, LP and LPV applications. K_V is set to 5.33 as defined in EUROCAE (2019).

Figure 2 illustrates the pre-processing steps before the computation of positions and protection levels in the DFMC SBAS explained above. The broadcast SBAS message type 31, 32, 34, 35, 36 and 37 indicates the healthy satellites that are allowed to be used for positioning purpose and for computation of the protection levels. For these augmented satellites, the major points allowing the SBAS corrections to be used are:

(1) The issue of data navigation (IODN) in the SBAS suggested message type 32 matches the issue of data, clock (IODC) for a GPS satellite in the L1 LNAV navigation message or the issue of data navigation (IODnav) for a Galileo satellite in the F/NAV navigation message;

(2) The issue of data mask (IODM) of the integrity messages matches one active satellite mask given in the suggested message type 31;

(3) The corresponding SBAS corrections (message type 32) and integrity information (message type 32, 34, 35, 36) used are within the time-out windows, which are pre-defined or computed based on parameters broadcast in the SBAS message (message 37);

(4) The DFREI (message type 32, 34, 35, 36) allows the usage of the corresponding corrections.

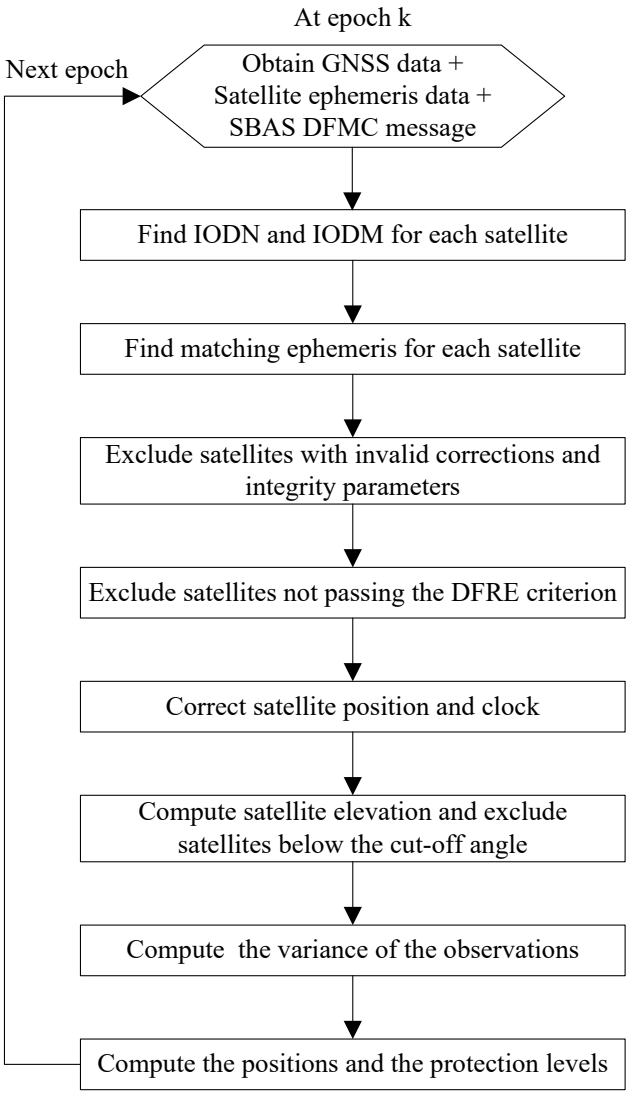

Fig. 2 Flowchart of the pre-processing procedure for computing the position and the protection levels using DFMC SBAS

4. Real-data analysis

In this section, 1 Hz data spanning DOY 257 to 268, 2018 (from September 14 to September 25, 2018) of two Australian stations, CUT0 and UWA0, was used as examples for the real data analysis. The two stations are equipped with TRIMBLE NetR9 and SEPT Polarx5 receivers, respectively. For the code-smoothing process, the smoothing time window was set as 100s for the ionosphere-free combination of the GPS L1/L2 and Galileo E1/E5a measurements. The elevation mask was selected as 5 degrees. Based on the requirements of LPV-200 (ICAO, 2009), the HPLs and the VPLs are examined with a Horizontal Alert Limit (HAL) of 40 m and a Vertical Alert Limit (VAL) of 35 m.

Within the test duration, the number of available satellites is 31 and 17 for GPS and Galileo, respectively. Figure 3 (top) gives the number of visible satellites above the mask angle at CUT0 as an example. The average number of satellites observed at any epoch for GPS and Galileo is about 10 and 5, and the daily repeatability of the GPS satellite numbers can be well observed.

Figure 3 (bottom) shows the number of satellites eventually used in the solution of the position and protection levels at CUT0. The number of Galileo satellites used is lower than that of GPS, partially due to its actual lower visibility at CUT0 (see top panel of Figure 3). Furthermore, at certain time epochs that are less than 1% of the total number of epochs, the number of Galileo satellites was zero due to the exclusion of satellites by the DFRE criterion. For example for the epoch 00:18:43 on 14 September (DOY 257) 2018, six Galileo satellites were observed at CUT0. However, the DFREI values were 15 for all the six satellites, which leads to their exclusion. Some GPS satellites were also excluded. For example, the GPS satellite PRN19 experienced an outage from 08:39 to 14:06 on September 14, 2018 (DOY 257) due to its unhealthy status as indicated in the navigation message. These epochs are not found to have significant influences on the overall positioning accuracy.

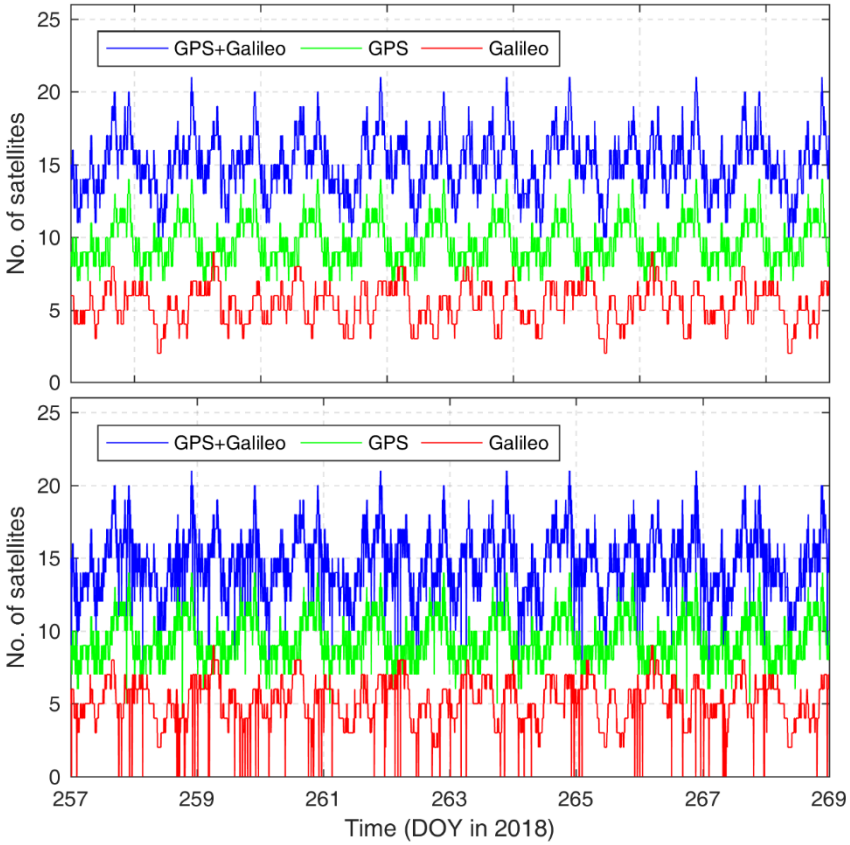

Fig. 3 Number of visible satellites above the mask angle (top) and number of the usable satellites for the DFMC SBAS service (bottom) at CUT0

The DFMC SBAS positioning errors are shown in the north, east and up directions in Figure 4 spanning DOY 257 to 268, 2018. The position error is computed as the difference between the estimated positions using the DFMC SBAS and the known position of the test stations. As can be seen, positioning errors have mean values close to zero. The positioning accuracies in the north and east directions are close to each other, better than that of the up direction.

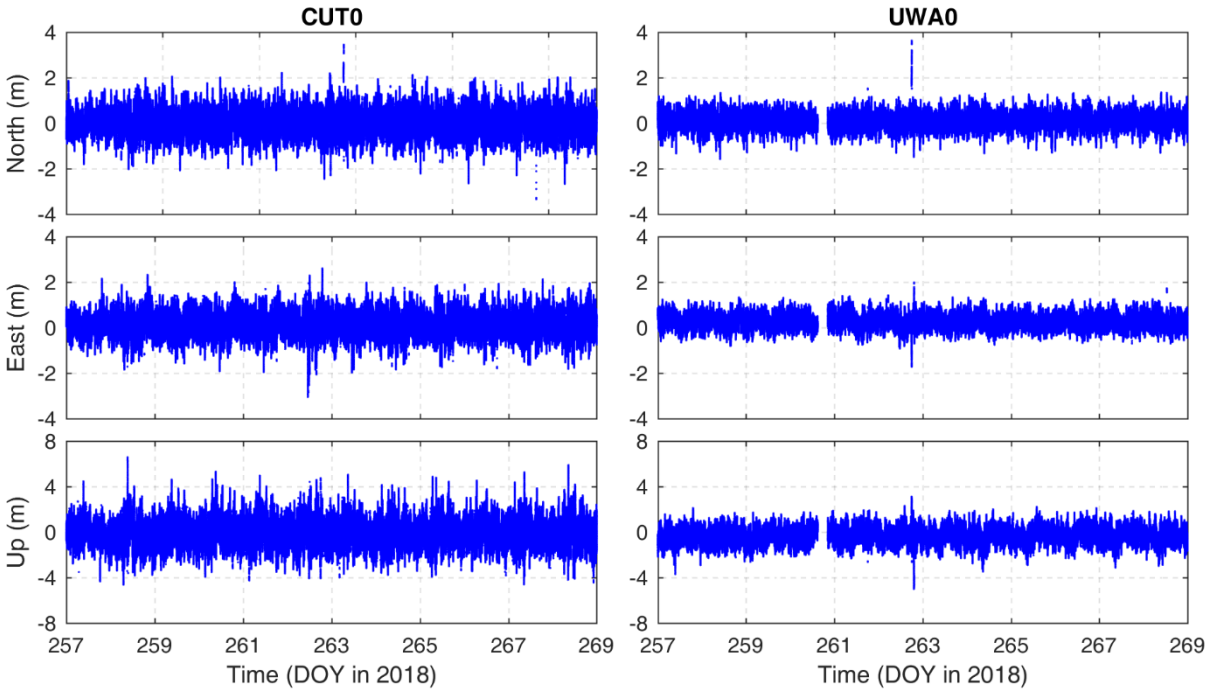

Fig. 4 The DFMC SBAS positioning errors at CUT0 (left) and UWA0 (right)

Figure 5 depicts the probability density function (PDF) of the normalized positioning errors, which generally follow a standard normal distribution. The corresponding descriptive statistics including the root mean square error (RMSE) and the standard deviation (σ) are summarized in Table 2. Recall that for the normal distribution, the probabilities of the observations within the 1 σ, 2 σ and 3 σ limits are 68.3%, 95.4% and 99.7%, respectively, which are similar to the statistics given in the last three columns of Table 2 based on the DFMC SBAS results. The small differences can be explained by errors like multipath. It is noted that the actual errors are not required to exactly follow the Gaussian distribution. They are only required to be bounded by the PLs, which assumes an over-bound of a Gaussian distribution of the errors.

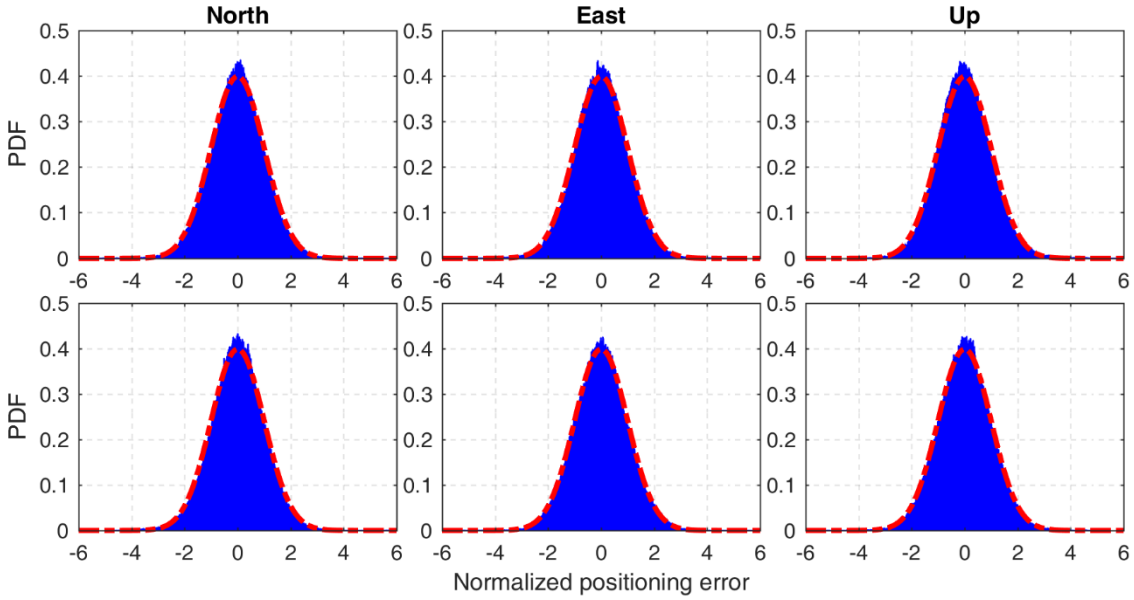

Fig. 5 The PDF of the DFMC SBAS normalized positioning errors in each direction at CUT0

(top) and UWA0 (bottom) compared with the formal ones (red dotted line).

Table 2 Descriptive Statistics of the DFMC SBAS positioning errors in each direction

Station	Component	RMSE(m)	σ(m)	Positioning error percentage w.r.t. the mean values		
				$<1\sigma$	$<2\sigma$	$<3\sigma$
CUT0	North	0.528	0.526	69.2%	95.4%	99.5%
	East	0.491	0.474	69.8%	95.4%	99.4%
	Up	1.085	1.081	70.1%	95.3%	99.3%
UWA0	North	0.347	0.336	70.1%	95.5%	99.5%
	East	0.394	0.293	68.9%	95.3%	99.7%
	Up	0.762	0.664	69.3%	95.5%	99.5%

Figure 6 illustrates the computed protection levels with respect to the *absolute* DFMC SBAS positioning errors for the stations CUT0 and UWA0 in the horizontal and vertical directions, which are denoted as HPE and VPE, respectively. The results show that the positioning errors are bounded by the PLs and the ALs in both directions throughout the entire test period. Note that the data collected is only used to show an indication of the expected new SBAS performance, but does not aim to verify the planned PHMI of 10^{-7}, as this would require a very long data set. The gap in Figure 6 (right) is due to the receiver outage at UWA0 from 15:00 to 20:24 GPST on September 17 (DOY 260), 2018.

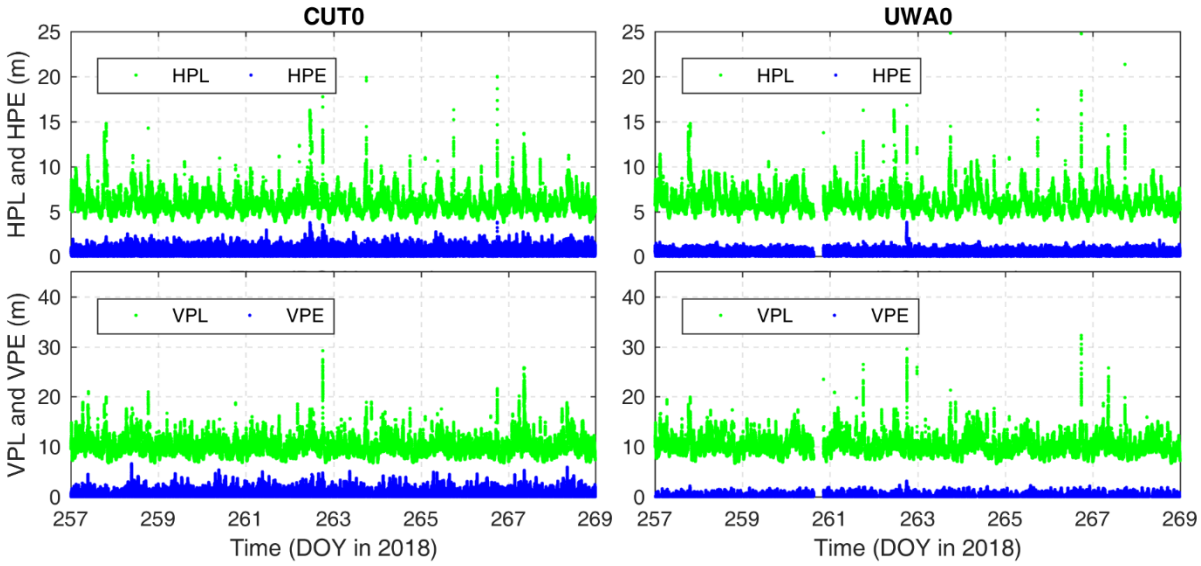

Fig. 6 Protection levels and the *absolute* positioning errors at CUT0 (left) and UWA0 (right)

As shown in Eq. (10), the variances of individual error sources are summed to form the total variance of the O-C observations and the weighting matrix, which in turn affects the PL and the consequent availability of IM. It is therefore essential to evaluate the contribution of the individual error sources on the protection levels. Each error source is influenced by different factors, and thus exhibits different characteristics. More specifically, the DFC residual errors

are related to the precision of the SBAS orbital and clock corrections in addition to the receiver-satellite relative geometry, whereas the other error sources are merely modelled as a function of the satellite elevation angles.

The contributions of different error sources to the protection levels at CUT0 are further presented in Figure 7 for HPL (top) and VPL (bottom). The figure shows that the protection levels are predominantly influenced by the DFC residuals (related to the orbital and clock errors). Airborne receiver errors consisting of the receiver noise, the multipath and the uncertainly of the antenna group delays are the second largest contributor. The tropospheric and ionospheric residuals play a secondary role and do not strongly vary within the entire time period. Recall that, the availability of IM can be measured as the ratio of time PL<AL compared with the entire time operation period. Therefore, it is of interest to keep the PL low as long as they bound possible positioning errors. Figure 7 clearly shows that to lower the PLs, to improve the availability of IM, it is necessary to reduce σ_{DFC}, and thus, its contribution in HPL. While as shown from the test, the results satisfy LPV-200 integrity requirements, where all HPL<40 m and VPL<35 m, it also suggests that an improved level of the SBAS satellite orbital and clock corrections would be needed if DFMC SBAS is considered for the more critical phases of precision approaches, which are expected from the next generation of satellites.

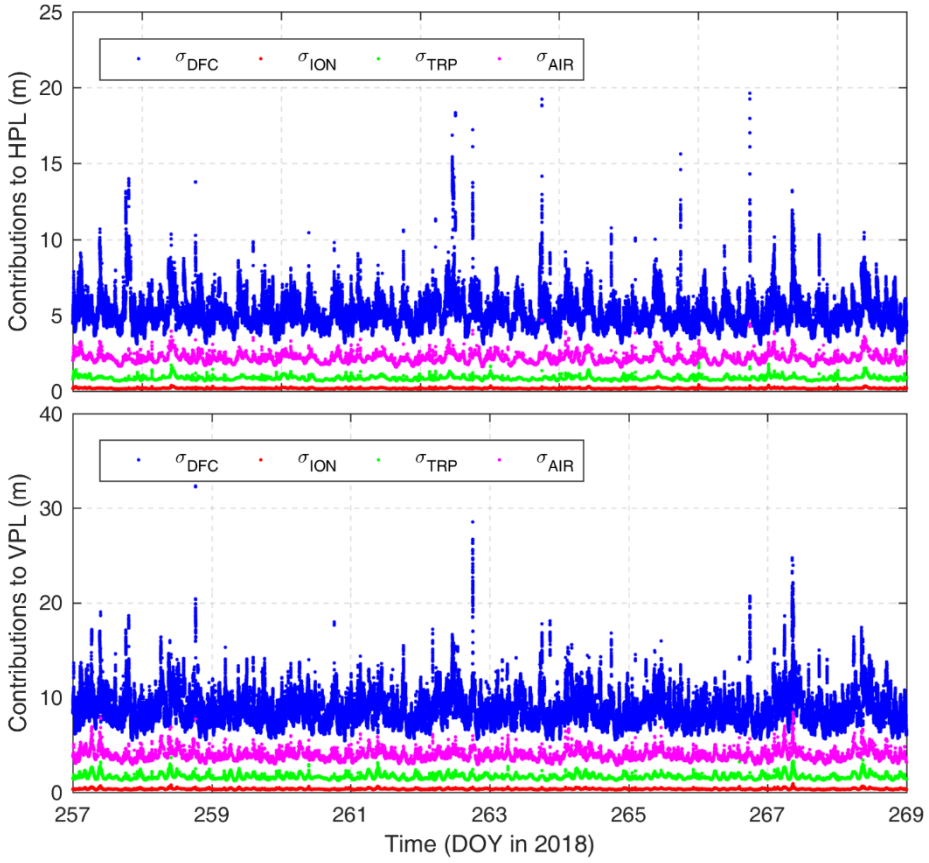

Fig. 7 Contributions of different errors to the HPLs (top) and the VPLs (bottom) at CUT0

5. Protection levels for the entire coverage area of the Australian DFMC SBAS

Different from the positioning errors that need to be computed based on real satellite observations at specific locations, the protection levels are only related to the geometry of

satellites observed (without their range measurements), and the variance-covariance matrix of the O-C observation terms, which can be derived from the SBAS message and the satellite geometry, in addition to the required PHMI. This allows us to compute and explore the variations of the protection levels on a larger scale at simulated regions where the DFMC SBAS can be acquired. Note that the real-data results presented in the previous section are based on the actual measurements collected at CUT0 and UWA0, whereas in this section all relevant satellites above the elevation mask are assumed to be observable, but again those which are approved by the SBAS service are used.

In this study, the area covering the Asia-Pacific region with the longitude from 60°E to 120°W and the latitude from 80°S to 80°N, is divided into 2°×2° grids. This is slightly wider than the foot-print of the GEO satellite Inmarsat-4F1, as a wider coverage area can be expected in the future when two GEO satellites are put into service in the final operational system. The protection levels are computed based on the broadcast ephemeris and the actual DFMC SBAS message from September 14 to September 25, 2018, with a mask angle of 5 degrees similar to the previous section. In this section, the analysis is focused on the VPLs, as the requirements on VPLs are always more constraining in aviation.

Figure 8 depicts a coloured scale of the average VPLs (left), the average number of satellites (middle) including both GPS and Galileo and the average vertical dilution of precision (VDOP) values (right) over the 12 days of the study. It can be seen that the average VPL values range between 8 m and 13 m. In general, the VPLs decrease with the increase in the number of observed satellites. The values in the equatorial region show good examples of this correlation. However, it is also observed that the average VPLs in most of the Asia-Pacific region are smaller than those in the regions close to the poles. This can be explained by Figure 8 (right), where it can be seen that the polar regions although having a higher average number of satellites shown in Figure 8 (right), they also have larger VDOP values, due to poorer satellite geometry, and the regions within latitude from 60°S to 60°N have the lower VDOP values with the exception of those lie in the northern Pacific Ocean.

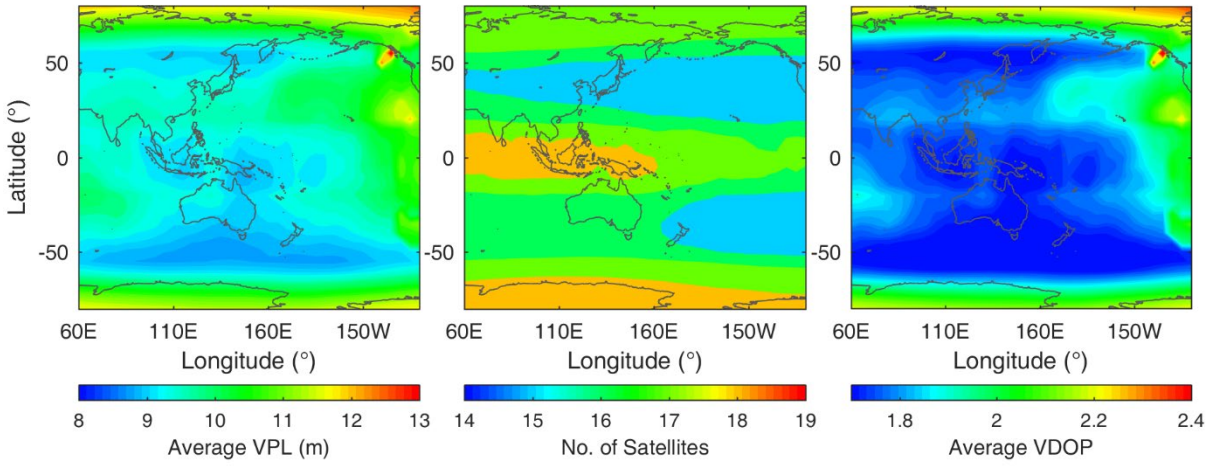

Fig. 8 The average VPLs (left), the average satellite numbers (middle) and the average VDOP (right) over the investigated area from September 14 to September 25, 2018

To demonstrate the relationship between the VPL computed by the new DFMC SBAS and

satellite numbers as well as VDOP, as an example, Figure 9 illustrates the maximum VPL (left), the corresponding satellite numbers (middle) and VDOPs (right) across the tested grid on September 14, 2018. The maximum VPL within entire Australia, New Zealand and surrounding waters, as well as most Asia-Pacific areas, are far below the VAL of 35 m, and thus reaching 100% IM availability and satisfying LPV-200 throughout the entire processing period during the test. The areas that have maximum VPL exceeding the VAL, showing in yellow and red in Figure 9 (left) is explained by the low observed number of satellites and the poor satellite geometry of this region, as shown in Figure 9 (middle and right).

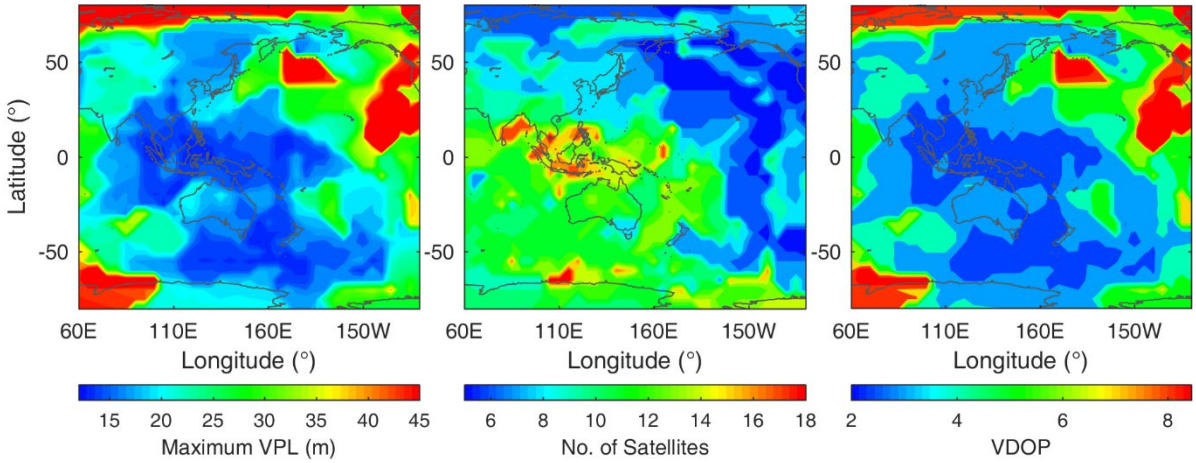

Fig. 9 The maximum VPL (left) at each grid point with the corresponding satellite numbers (middle) and VDOPs (right)

6. The impact of mask angle and technology trend of DFMC SBAS

The mask angle directly affects the number of satellites used for positioning and computation of the PLs. In this section, the impact of the mask angle is investigated in different scales. Figure 10 depicts the VPL of CUT0 on September 14, 2018, with different mask angles. From the result, it becomes clear that the larger mask angle will trigger the increase of VPL of the new DFMC SBAS.

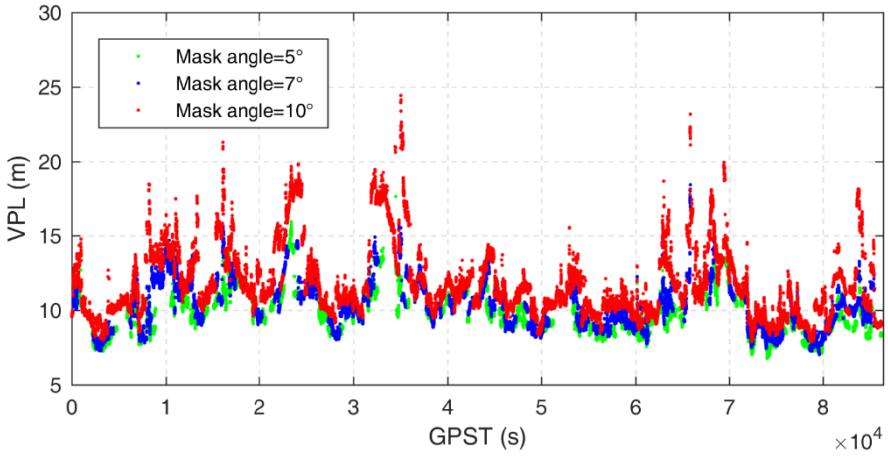

Fig. 10 VPL of CUT0 on September 14, 2018, with different mask angles

In order to experimentally demonstrate the effect of the mask angle at simulated regions, the

integrity availability, i.e. the percentage of epochs when VPL<VAL compared with the total number of epochs, was computed by using three different mask angles, namely 5°, 7° and 10° as shown in Figure 11.

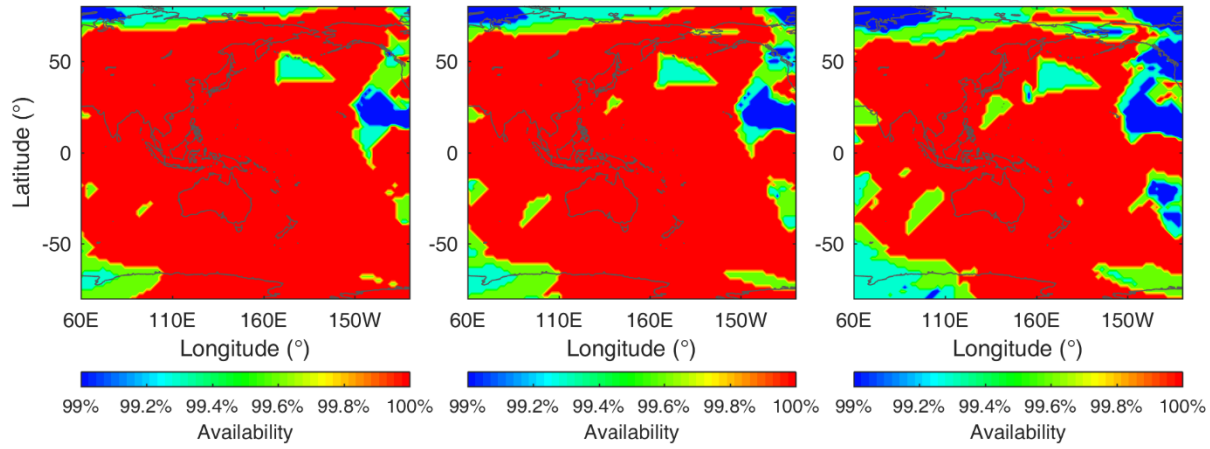

Fig. 11 Availabilities of IM using mask angles 5° (left), 7° (middle) and 10° (right) on September 14, 2018

Figure 11 confirms that integrity availability tends to shrink with the increase of the mask angle due to a reduction in the number of the satellites used. The percentage of grids with 100% IM availability amounts to 86.2%, 81.2% and 71.3% for 5°, 7° and 10° mask angle, respectively. Note that the LPV-200 is critical for precise approaches close to CAT I at airports. One can see that these areas of main interest to Australia, New Zealand, most Asia-pacific and their surrounding waters have 100% IM availabilities in all cases during this preliminary test.

As mentioned before, the DFC residual errors have the largest contribution to the majority of the protection levels. Therefore, improving the precision of the DFC is essential for obtaining lower protection levels and achieving higher integrity availabilities, if DFMC SBAS is considered for higher categories in the future, e.g. for CAT II. Of course, this is just one aspect in this regard. To simulate the impact of using more precise SBAS orbital and clock corrections, comparisons were performed with a mask angle of 5° and with the DFREI reduced by different values. This may happen in the future with the improvement in the computation of the satellite ephemeris, GPS moving to Block III, improved satellite capability and improved the ground monitoring network, and processing software. Figure 12 shows the VPL of CUT0 on September 14, 2018, with differently reduced DFREI values.

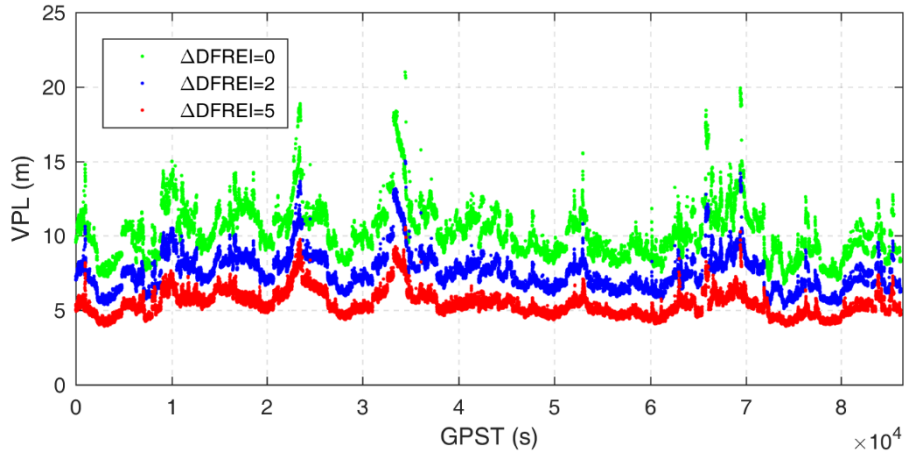

Fig. 12 VPL of CUT0 on September 14, 2018, with DFREI reduced by different values

Figure 12 demonstrates the reduced DFREI will help to improve the VPL performance profoundly, which is expected in the near future. Figure 13 shows the IM availabilities at simulated regions on September 14, 2018, under LPV-200. Comparing the last two plots to the first one in Figure 13, a clear improvement can be perceived in the IM availabilities when reducing the DFREI. The percentage of grids with 100% availability increases from 86.3% to 93.9% and 97.6% with the DFREI reduced by 2 and 5, respectively.

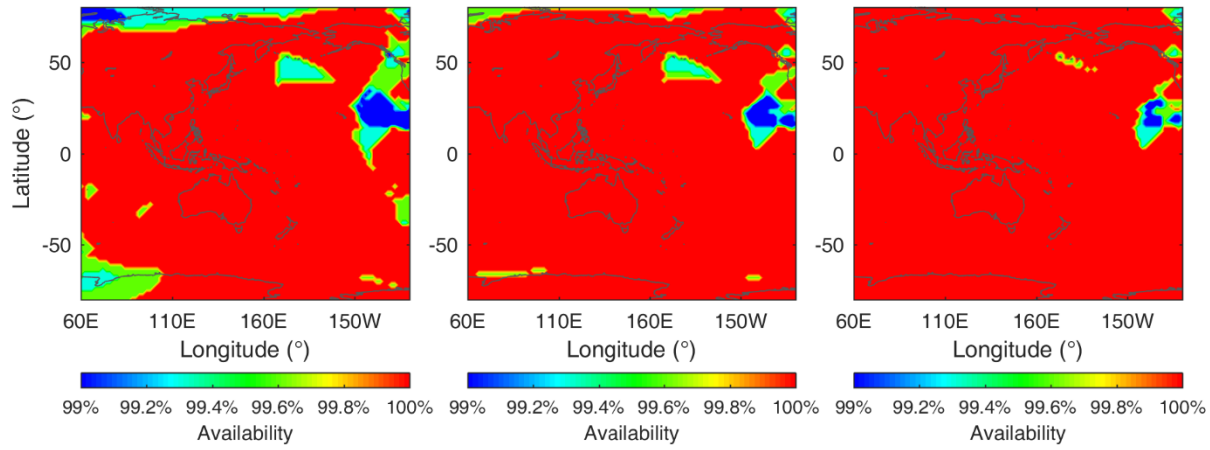

Fig. 13 IM availability for a mask angle of 5° with the DFREI reduced by 2 (middle) and reduced by 5 (right) compared to the original DFREI (left) on September 14, 2018

Finally, the analysis in this study is performed based on the GPS L1/L2 signals due to the currently limited number of GPS IIF satellites. Moreover, at present, the Galileo constellation has a low number of satellites. In the future, with more Galileo and switching to GPS III satellites transmitting L5 signals, and with the expected improvement in the precision of the SBAS corrections, achieving close to 100% IM availability can be expected over the entire Asia-pacific region if SBAS is available all the time and maintain the same level as the tested one.

7. Conclusion

DFMC SBAS is the future of SBAS. This new generation of SBAS is immune to the first-order ionospheric delays and has an expanded service coverage area compared to the legacy SBAS L1 service. This work presents a preliminary study showing the results of the integrity performance using the Australia and New Zealand SBAS test-bed with a focus on the LPV-200 applications. The DFMC SBAS protection levels are analyzed based on *real SBAS messages* at two stations and a simulated grid over the entire Asia-pacific region.

Currently, the number of available satellites is higher for GPS than for Galileo. Using the dual-frequency GPS and Galileo data of two static stations located in Australia, the RMSE of the DFMC SBAS results are at the sub-meter to meter level, and the absolute horizontal and vertical positioning errors were always bounded by the HPLs and VPLs over the entire test time period. The HPLs and VPLs were also below HAL and VAL of the LPV-200. The analysis shows that among all the error sources, the DFC residual errors play a prominent role in the computation of the HPLs and VPLs.

The simulations of the VPLs were performed over the entire Asia-Pacific area based on the broadcast ephemeris and the SBAS message over twelve consecutive days in 2018, which would give representative conclusions taken into consideration the repeatability of satellite orbits. Using a 5° mask angle and $PHMI_V$ allocated within the total PHMI of 10^{-7}, average VPL values ranging between 8 m and 12 m were obtained. In general, the VPLs decrease with the increase in the number of observed satellites and with the improvement in their geometry. Hence, VPLs in most of the mid-latitude Asia-Pacific regions were smaller than those in the regions close to the poles. The maximum VPL across most of the main area of interest was below a VAL of 35 m throughout the entire processing period even when the mask angle was increased to 10°, and thus reaching 100% IM availability during the test and satisfying LPV-200 requirement in this regard. Even better performance is expected in the future, assuming continuous availability of DFMC SBAS, with more Galileo satellites and the use of GPS Block III satellites, and with the expected improvement in the precision of SBAS corrections.

Acknowledgements

This work was supported by the ARC Discovery Project: Trustworthy Positioning for Next Generation Intelligent Transport Systems, Project ID: DP170103341, and the Jiangsu Government Scholarship for Oversea Studies in 2018, and the National Natural Science Foundation of China (No.41504024). The authors would like to thank the GMV Company (Spain) for providing the decoded DFMC SBAS messages used in the tests. The raw GNSS data was obtained from http://saegnss2.curtin.edu/ldc/. We thank the University of Western Australia for hosting the station of UWA0, and Septentrio for providing the receiver at UWA0.

References:

Blanch J, Walter T, Enge P (2005) Protection level calculation using measurement residuals: theory and results. In: Proceedings of ION GNSS 2005, Long Beach, CA, September 2005, pp 2288-2296

Bunce D. (2014) Wide Area Augmentation System (WAAS) Status and History. https://www.gps.gov/multimedia/presentations/2014/09/ION/bunce.pdf

Barrios J, Caro J, Calle J, Carbonell E, Pericacho J, Fernández G, Esteban V, Fernández M,

Bravo F, Torres B, Calabrese A, Diaz A, Rodríguez I, Laínez M, Romay M, Jackson R, Reddan P, Bunce D, Soddu C (2018) Update on Australia and New Zealand DFMC SBAS and PPP System Results. In Proceedings of ION GNSS+ 2018, Miami, Florida, September 24-28, 2018, pp.1038-1067

Choy S, Kuckartz J, Dempster AG, Rizos C, Higgins M (2017) GNSS satellite-based augmentation systems for Australia. GPS Solutions, 21:835-848. doi:10.1007/s10291-016-0569-2

Deo M, Twilley B (2008) The South Pacific Regional GNSS Network. Integrating Generations FIG Working Week 2008 Stockholm, Sweden, 14-19 June 2008

El-Mowafy A, Yang C (2016) Limited sensitivity analysis of ARAIM availability for LPV-200 over Australia using real data. Advances in Space Reserch, 57(2):659-670. doi:10.1016/j.asr.2015.10.046

El-Mowafy A, Cheung N, Rubinov E (2019) First results of using the second generation SBAS in Australian Urban and Suburban Road Environments. Journal of Spatial Science, 65(1):99-121. doi: 10.1080/14498596.2019.1664943.

EUROCAE (2019) Minimum Operational Performance Standard for Galileo/Global Positioning System/ Satellite-Based Augmentation System Airborne Equipment. EUROCAE ED-259,01/02/2019 (EUROCAE, Paris 2019)

Geoscience Australia (2017) Satellite Based Augmentation System test-bed project. https://www.ga.gov.au/scientific-topics/positioning-navigation/positioning-for-the-future/satellite-based-augmentation-system (Accessed on 11 September 2019)

Grunwald G, Bakuła M, Ciećko A (2016) Study of EGNOS accuracy and integrity in eastern Poland. The Aeronautical Journal, 120(1230): 1275-1290. doi:10.1017/aer.2016.66

ICAO, A. 10 (2009). GNSS standards and recommended practices (SARPs). Section 3.7, Appendix B, and Attachment D, Aeronautical Telecommunications, 1.

Johnston G, Riddell A, Hausler G (2017) The International GNSS Service. In Teunissen PJG, Montenbruck O (eds), Springer Handbook of Global Navigation Satellite Systems (1st ed, pp. 967-982). Springer International Publishing, Cham, Switzerland. doi: 10.1007/978-3-319-42928-1

LINZ (2020) PositioNZ, Land Information New Zealand. https://www.linz.govt.nz/data/geodetic-services/positionz (Accessed on 11 May 2020)

Pireaux S, Defraigne P, Wauters L, Bergeot N, Baire Q, Bruyninx C (2010) Higher-order ionospheric effects in GPS time and frequency transfer. GPS solutions, 14(3): 267–277. doi:10.1007/s10291-009-0152-1

Roturier B, Chatre E, Ventura-Traveset J (2001) The SBAS integrity concept standardised by ICAO. Application to EGNOS.Navigation-Paris 49, 65–77.

RTCA (2016) Minimum Operational Performance Standards for Global Positioning System/Wide Area Augmentation System Airborne Equipment, RTCA DO229E, 15/12/2016 (RTCA, Washington DC 2016)

Salos D, Vuillaume J, Kanj A, Dufour F, Suard N, Boulanger C (2018) Up-to-date DFMC SBAS service volume prototype (DSVP) to support DFMC performance characterization activities. In: 2018 European Navigation Conference, Gothenburg, Sweden, May 2008, pp 112–120

Teunissen PJG, Montenbruck O (eds) (2017) Springer handbook of global navigation satellite

systems. Springer, Berlin. .doi:10.1007/978-3-319-42928-1
Twilley RJ, Digney PW (2001) The Australian regional GPS network. Physics and Chemistry of the Earth, Part A: Solid Earth and Geodesy, 26(6-8): 629-635. doi: 10.1016/S1464-1895(01)00112-0
Walter T, Blanch J, Enge P (2007) L5 satellite based augmentation systems protection level equations. In: Proceedings of the International GNSS conference, Sydney, Australia, December 2007, pp 1–11
Walter T, Blanch J, Enge P (2010) Vertical protection level equations for dual frequency SBAS. In: Proceedings of ION GNSS 2010, Portland, OR, September 2010, pp 2031–2041
Walter T, Blanch J, Eric Phelts R, Enge P (2012a) Evolving WAAS to Serve L1/L5 Users. Navigation, 59(4): 317–327. doi:10.1002/navi.21
Walter T, Blanch J, Enge P (2012b) L1/L5 SBAS MOPS to support multiple constellations. In: Proceedings of ION GNSS 2012, Nashville, TN, September 2012, pp 1287–1297
Walter T, Blanch J, Enge P (2014) Reduced subset analysis for multi-constellation ARAIM. In: Proceedings of ION ITM 2014, Institute of Navigation, San Diego, California, Jan 2014, pp 89–98
Wanner B, DeCleene B, Nelthropp D, Gordon S (2008) Wide Area Augmentation System vertical accuracy assessment in support of LPV-200 requirements. Navigation 55(3): 191–203. doi:10.1002/j.2161-4296.2008.tb00429.x
Wang K, El-Mowafy A, Khaki M, Sutherland T, Rubinov E (2020) Assessment of the New DFMC and PPP services of the second-generation SBAS in the Mining and Urban environments. In the proceedings of the International Global Navigation Satellite systems (IGNSS) 2020, No. 49, 1-15, Sydney, Australia, 5-7 February.
Zumberge JF, Heflin MB, Jefferson DC, Watkins MM, Webb FH (1997) Precise point positioning for the efficient and robust analysis of GPS data from large networks. Journal of Geophysical Research, Solid Earth, 102(B3):5005–5017. doi: 10.1029/96JB03860